Check for updates

Water-triggered synergistic fluorescence variation and shape deformation in a Zn-TCPP metal–organic framework-based gel†

Xiangnan Wang,[a] Zeyu Feng,[a] Congyang Ye,[a] Haofeng Zang,[b] Yonghua Lu,[b] Hongli Zhang*[a] and Gang Zou [ID] *[a]

Smart materials with programmable shape deformation and synergistic shape/fluorescence variation are highly desired in various practical applications, such as bio-inspired multifunctional robots and machines. However, it is still quite challenging to construct smart surfaces with dynamic fluorescence and morphology from MOFs, which potentially introduce superior performance. Herein, we proposed to utilize Zn-TCPP MOFs and polyurethane to construct a smart hybrid gel, which could exhibit synergistic dynamic fluorescence and reconfigurable patterns upon treating with pure water. Their reversible fluorescence variation as well as the swelling of the surface could be observed even directly by the naked eye. Based on the above results, we designed a dual-response rewriting pattern and flower-like artificial actuator with simultaneous fluorescence variation and shape deformation performance. This study would be of great fundamental value in the rational design of novel smart materials and surfaces.

Introduction

In nature, many organisms exhibit interesting mechanical deformation as well as color or fluorescence change upon external stimuli, for the purpose of transmitting information or self-protection.[1–7] Inspired by these marvelous multifunction synergistic behaviors of natural systems, numerous artificial smart materials and surfaces have been widely studied due to their unique properties and various potential applications in actuators,[8] optoelectronics,[9–11] energy storage devices[12–14] and so on. Among them, the combination of luminescent materials and polymer gels can develop biotissue-like mechanical properties, which have been used to replicate the synergistic dynamic fluorescence and reversible shape deformation behaviors. For example, Wu *et al.* presented a tough hydrogel with good shape-memory ability and photo-tunable emission behaviors, affording reprogrammable shape designing and information encoding for dual-encryption.[15] Chen *et al.* reported aggregation induced emissive carbon dot gels for octopus-inspired shape/color synergistic adjustable actuators.[16] Compared to traditional dyes and quantum dots,

luminescent metal–organic frameworks (MOFs) have several intrinsic advantages such as highly tunable luminescence and structural diversity.[17–21] However, few luminescent MOFs have been utilized to construct artificial smart surfaces allowing response to external stimuli, and exhibition of tunable fluorescence and shape deformation.

In the past decades, MOFs have been deemed as potential function materials for molecular detection, gas storage and separation, and sensors[22] due to their distinctive advantages including stable structure, tunable porosity, ease of functionalization, and luminescent nature.[23–28] Porphyrins are commonly used MOF modules which have large and rigid three-dimensional special structures; thus, great efforts have been made to construct the sensors for sensitive detection of ions[29–34] and small molecules[35–39] based on the fluorescence changes of metal porphyrins. Since most MOFs are not as malleable as soft materials due to their crystalline nature, they are difficult to directly utilize as artificial smart materials that undergo mechanical deformation accompanied by fluorescence variation. On the other hand, water as a widespread substance participates in a variety of chemical and physical processes. The dynamic wetting process was usually utilized to induce the shape deformation of soft robots and actuators.[16] However, water hardly affected the fluorescence performance of the porphyrins. It still remains a challenge to construct MOF-based smart materials with synergistic dynamic fluorescence and reversible shape deformation behaviors during a dynamic wetting–drying process. Moreover, their intrinsic correlation

a Department of Polymer Science and Engineering, University of Science and Technology of China, Hefei, Anhui 230026, P. R. China.
E-mail: gangzou@ustc.edu.cn, zhl1992@ustc.edu.cn

b Department of Optics and Optical Engineering, University of Science and Technology of China, Hefei, Anhui 230026, P. R. China

and the rational design strategy of novel smart materials therefore remain undeveloped.

Herein, we reported a water-triggered dual-response Zn-TCPP/polyurethane gel to construct a synergistic dynamic fluorescence and shape deformation functional film. The mechanism of the water-triggered fluorescence enhancement was demonstrated and the effect of water content on fluorescence intensity was described in detail. What's more, a rewritable word pad was designed based on the reversible stimulus response properties and an opening–closing and fluorescence change clover device was constructed to simulate the morphological and color changes of natural organisms. This study provided an elegant strategy for developing novel smart materials for application in artificial muscles and soft robots.

Experimental

Materials and instruments

Meso-tetra(4-carboxyphenyl)porphine (TCPP, 95%) was obtained from Leyan Co. Ltd. Pyrazine (99%) was obtained from Aladdin Co. Ltd. Zinc nitrate hexahydrate (99%), polyvinylpyrrolidone (PVP K30, GR), N,N-dimethylformamide (DMF, 99.5%), ethanol (99.7%) and tetrahydrofuran (THF, 99.5%) were obtained from Sinopharm Chemical Reagent Co. Ltd. Polyurethane (PU, HydroMed D4) was obtained from AdvanSource Biomaterials Co. Ltd. Ultrapure water was prepared by using a Synergy UV water purification system. All the reagents and solvents were used as received without any further purification.

The SEM-EDS images were recorded using a GeminiSEM 500. Steady-state fluorescence measurements were obtained on a Hitachi F-4600 fluorescence spectrophotometer at room temperature. The white light photos were taken under a white light lamp. The fluorescence photos were taken by the camera loaded with a 500 nm filter under the illumination of a 405 nm laser (ZF-5, 8 W, 405 nm or 50 W, 405 nm). XPS was performed on a ESCALAB 250Xi X-ray photoelectron spectrophotometer. XRD was performed on a Rigaku TTR-III. LSCM was performed on an Olympus FV300. Ultraviolet-visible (UV-vis) absorption spectra were measured using a SHIMADZU UV-2700 PC spectrophotometer. FT-IR spectra were measured using a BRUKER TENSOR II.

Synthesis

Preparation of 2D Zn-TCPP. $Zn(NO_3)_2 \cdot 6H_2O$ (18.0 mg, 0.061 mmol) and PVP (80.0 mg, 1.00 mmol) were dissolved in a mixture of DMF (36.0 mL) and anhydrous ethanol (12.0 mL) in a tube. Then TCPP (16.0 mg, 0.020 mmol) and pyrazine (0.8 mg, 0.01 mmol) were dissolved in the mixture of DMF (36.0 mL) and ethanol (12.0 mL). The TCPP solution was added dropwise in the tube under stirring and ultrasonication for 15 min. The mixture was heated up to 80 °C and then maintained for 14 h. The resulting precipitate was washed consecutively twice with anhydrous ethanol and collected by centrifugation. Finally, the 2D Zn-TCPP was stored in ethanol.

The concentration of the dispersion was obtained by weighing the solid after dried in a vacuum oven at 65 °C for 30 h.

Preparation of the Zn-TCPP/polyurethane hybrid gel. 2D Zn-TCPP (1.0 mg) was dispersed in tetrahydrofuran (THF, 2.0 mL) via ultrasonication for 0.5 h. Polyurethane (200 mg) was added with stirring until it completely dissolved. The solution was dropped on the glass sheet and dried in air for 1 h. The formed film was further drying in a vacuum oven at 80 °C for 4 h.

Results and discussion

Firstly, we synthesized 2D Zn-TCPP MOF as shown in Scheme 1(a) according to a previous report.[40] The successful synthesis of the 2D Zn-TCPP MOF was proved by scanning electron microscopy energy dispersive spectroscopy (SEM-EDS) (Fig. S1, ESI†), X-ray photoelectron spectroscopy (XPS) (Fig. S2, ESI†) and X-ray diffraction (XRD) (Fig. S3, ESI†). The sheet structure of 2D Zn-TCPP MOF could be clearly seen through SEM images, and the scale of the sheet was about 2 μm. Besides, the existence of C, N, O and Zn was proved by EDS and XPS. The characteristic peaks at 284.8, 400.02, 532.15 and 1022.1 eV in XPS spectra were ascribed to C1s, N1s, O1s and Zn2p3 of the Zn-TCPP MOF. As shown in the Fig. S3 (ESI†), as-prepared Zn-TCPP MOF powder exhibited various strong diffraction peaks at 2.3°, 3.8° and 18.0°, respectively, indicating the formation of ordered structure of the MOF and the successful metallization (Zn^{2+}) of porphyrin. Through the above evidence, Zn-TCPP MOF was successfully synthesized. The synthesized MOF was stored in ethanol.

To achieve our idea of constructing MOF based smart materials, the functional film was prepared by dropping the MOF-PU mixture on the glass. In fact, the expansion of polyamides in water has been widely reported.[41,42] A commercial polyurethane named HydroMed D4 that is an ether-based hydrophilic polyurethane was selected as the substrate. The amide and ether bonds in polyurethane were observed using FT-IR spectra (Fig. S4, ESI†). The MOF was configured into a 1 mg mL^{-1} THF dispersion, then the polyurethane was added and stirred until completely dissolved into a 200 mg mL^{-1} viscous liquid. The viscous mixture was applied to the clean glass via a dropping film method. Finally, the prepared film was dried at room temperature in the air for 1 h, and remained in a vacuum oven at 80 °C for 4 h. To match the common light sources and the excitation light of the functional film, a 405 nm laser was used as the light source for taking fluorescence photos. Before the fluorescence test, the film was soaked in ultrapure water for 3 min and vacuum dried for 4 h. The prepared film is shown in the Fig. S5 (ESI†). No obvious change in the UV-vis spectra was observed before and after water treatment (Fig. S6, ESI†).

Interestingly, the functional film could respond to water stimuli. Under the activation of water, the film swelled and the fluorescence intensity increased significantly. After drying, the surface morphology and fluorescence intensity returned to the original state (Scheme 1(b)). The characteristic emission
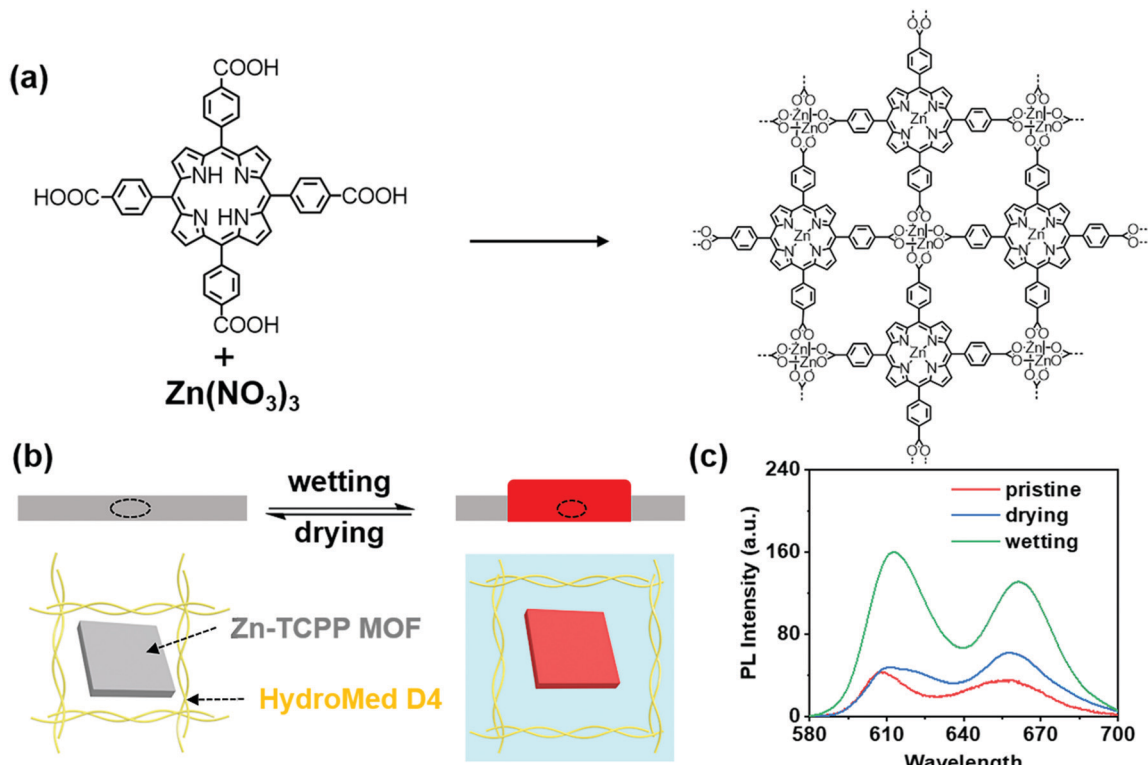
Scheme 1 (a) Synthesis of 2D Zn-TCPP. (b) Schematic illustration of the synergistic shape and fluorescence changes of the polyurethane-MOF film by water and the involved mechanisms. (c) Fluorescence spectra of Zn-TCPP MOF in the pristine state, dry state and wet state. All fluorescence tests were carried out under 405 nm light excitation.

peaks of zinc porphyrin at 610 nm and 660 nm are shown in the fluorescence spectra. Compared with the 1 mg mL^{-1} MOF aqueous dispersion (Fig. S7, ESI†), the prepared films had stronger emission, and the emission peak had a slight blue shift, which might be caused by aggregation caused quenching in aqueous dispersion. After wetting with ultrapure water for 3 min, the fluorescence intensity of the film became 2–3 times stronger than that in the dry state, and the emission peak redshifted slightly, which might be caused by the hydrogen bond interaction of water-amide-porphyrin affecting the PET effect (Scheme 1(c)). Thus, the fluorescence intensity of the MOF-polyurethane functional film was reversibly changed by a dynamic wetting–drying process. In order to verify the mechanism of fluorescence enhancement, we measured the fluorescence lifetime of the newly prepared film and the film after water treatment. The fluorescence lifetime is significantly improved (from t_{avg} = 0.27 ns to t_{avg} = 1.7 ns) (Fig. S8, ESI†), which was similar to previous literature reports.[43,44] To further investigate the interaction of hydrogen bonds, we compared the FT-IR spectrum of the film before and after water treatment (Fig. S9, ESI†). There was a red shift and broadening of the urethane carbonyl peak in the wetting film, indicating the formation of hydrogen bonds upon water treatment.[45] Above all, we successfully proved that the mechanism of fluorescence enhancement was mainly due to the hydrogen bonding between water, amide and porphyrin, which weakened the PET effect of zinc porphyrin.

As shown in Fig. 1(a), the prepared films emitted red fluorescence under 405 nm laser illumination. The fluorescence photos of the film demonstrated that the MOF was evenly dispersed in polyurethane. We used a camera equipped with a 500 nm filter to record the fluorescence changes of the film. When a blob of ultrapure water was dropped on the film, the fluorescence intensity at the wet part increased rapidly to 2–3 times that of the previous dry state within three minutes; for a wet film with strong the fluorescence would decrease continuously within half an hour by drying in a vacuum oven at 80 °C and entered the equilibrium state in 4 h (Fig. 1(b)). Significantly, drying under vacuum was necessary because possible oxidation occurred within the hybrid films, resulting in the irreversible water-induced fluorescence variation and shape deformation. Drying at 80 °C was done mainly considering the efficiency of dehydration and the ageing temperature of the polyurethane. In order to reveal the effect of water content on fluorescence, ethanol–water mixtures with different ratios were applied on the same film and then optical photo and fluorescence studies were carried out. The fluorescence intensity of the film increased gradually when the water content increased from 5% to 20%, and then flattened out from 20% to 100% (Fig. 1(c)). In addition, the emission intensity at 610 nm of the films showed good repeatability in multiple wetting–drying cycles (Fig. 1(d)), which manifests the reversible stimulus response properties of the film. It should be noted here that the fluorescence intensity could not return to the original value
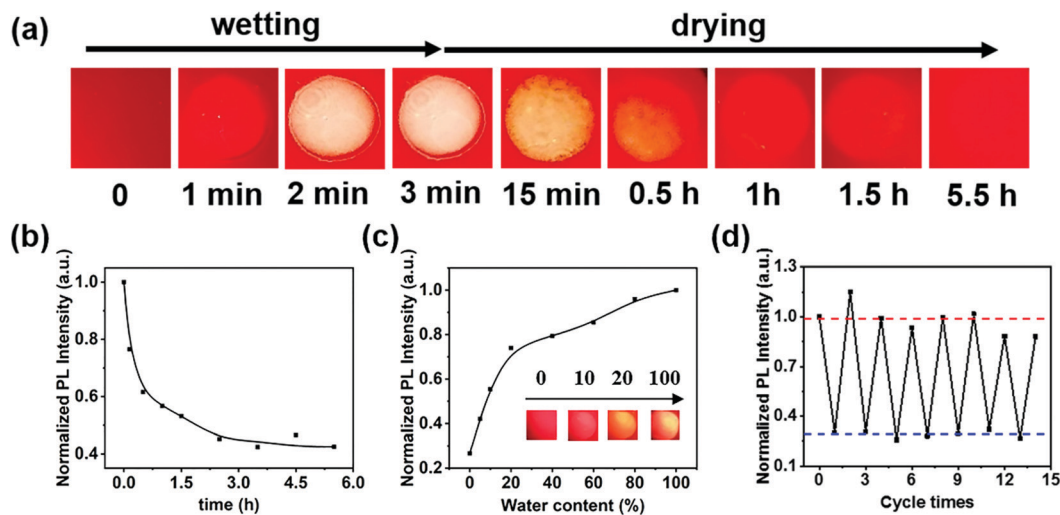
2116 | *Mater. Chem. Front.*, 2022, **6**, 2114–2121

This journal is © The Royal Society of Chemistry and the Chinese Chemical Society 2022

Fig. 1 (a) Fluorescence photos of watering−dehydration of the film from the dry state. (b) Heating time dependent fluorescence decay of the gelation state. (c) Fluorescence intensity and photos of the film at different water−ethanol ratios. (d) Fluorescence intensity under a wetting−dehydration cycle. All fluorescence tests were carried out under 405 nm light excitation, the fluorescence intensities were taken at 610 nm, the fluorescence photos were taken using a 500 nm filter loaded on the mobile phone.

(only 85% recovery). However, in the wetting–dehydration cycle process, the normalized fluorescence intensity in the dry state remained 0.29 ± 0.02, and those in the wet state remained 0.98 ± 0.09. Moreover, the hybrid films exhibited excellent fluorescence stability at suitable pH, temperature and solvent conditions, as shown in Fig. S10 (ESI†).

After studying the fluorescence properties of the material, it is necessary to further exhibit their surface difference. Writing on the surface of the functional film with ultrapure water could realize the naked eye visible pattern. Note that some ions might be present on the writing brush and must be removed by ultrasonic washing three times with ultrapure water before use. After leaving an A-shaped water mark, the excess water was wiped off after waiting for three minutes. An obvious A-shaped protrusion could be seen by naked eye under the white light; also the bright letter "A" could be seen using a 500 nm filter under the illumination of a 405 nm laser. After dehydration, it was basically restored to its original state, and no obvious trace could be seen under the same white light or 405 nm laser illumination (Fig. 2(a)).

Moreover, the fluorescence difference between the wet and the dry state could be recorded by laser scanning confocal microscope (LSCM). We used a micro injector as the brush to draw a water line on the film. After 3 minutes, an obvious bright line could be observed under the microscope (Fig. 2(b)). After vacuum dehydration, the bright linear pattern disappeared. An optical microscope and step profiler were used to characterize the height difference between the dry and wet states. As depicted in Fig. 2(c), no obvious microstructure difference was observed between the wet position and the dry position through the microscope, but a boundary line could be clearly seen. Besides, the evenly dispersed MOF layer in the polymer could further demonstrated by an optical microscope. The step profiler analysis for the wet part showed that it

protruded about 51 μm from the surface. The expansion part was usually gradual, and the boundary was a gradual slope. Sharp protrusions might be caused by dust (Fig. 2(d)).

Based on the above results, the Zn-TCPP MOF gel could be successfully prepared, and its water-triggered synergistic fluorescence and shape deformation variation performances have been known to us. Due to the easy operation and reversibility of the novel gel material, further exploring the excellent applications are highly desired. Fortunately, a rewritable word pad was successfully designed. The mechanism of the word pad was represented by simulation (Fig. 3(a)). After scribbling on the substrate using a water-bearing brush, a letter gradually protruded from the plane, and the bright letter also appeared under the illumination of a 405 nm laser. Next, the word "D", "R" and "Y" was displayed in the same position of the film in turns after drying and rewriting through fluorescence photos using a 500 nm filter and white light photos (Fig. 3(b)). When the letter "D" was written with water, the obvious D-shaped bulge could be seen by the naked eye under white light, and the bright letter "D" could also be seen under 405 nm illumination. After 80 °C vacuum drying, the traces of letters could hardly be seen both under 405 nm laser and under white light. In this case, the surface of the film was nearly flattened, and the fluorescence intensity of the writing part was nearly reduced to that of the background. After that, the letters "R" and "Y" were written in the same position and then erased in turn. The writing–erasing cycle study showed the macro dynamic word "DRY" in the same position, which was also the name of the erasing process. These erasable multi-level patterns might have wide application prospects in information transmission.

As we all know, many plants show interesting appearance changes due to the stimulation of the ecological environment in nature. A typical example is *Hibiscus mutabilis L.* The color of *Hibiscus mutabilis L.* petals is as white as snow in the morning,
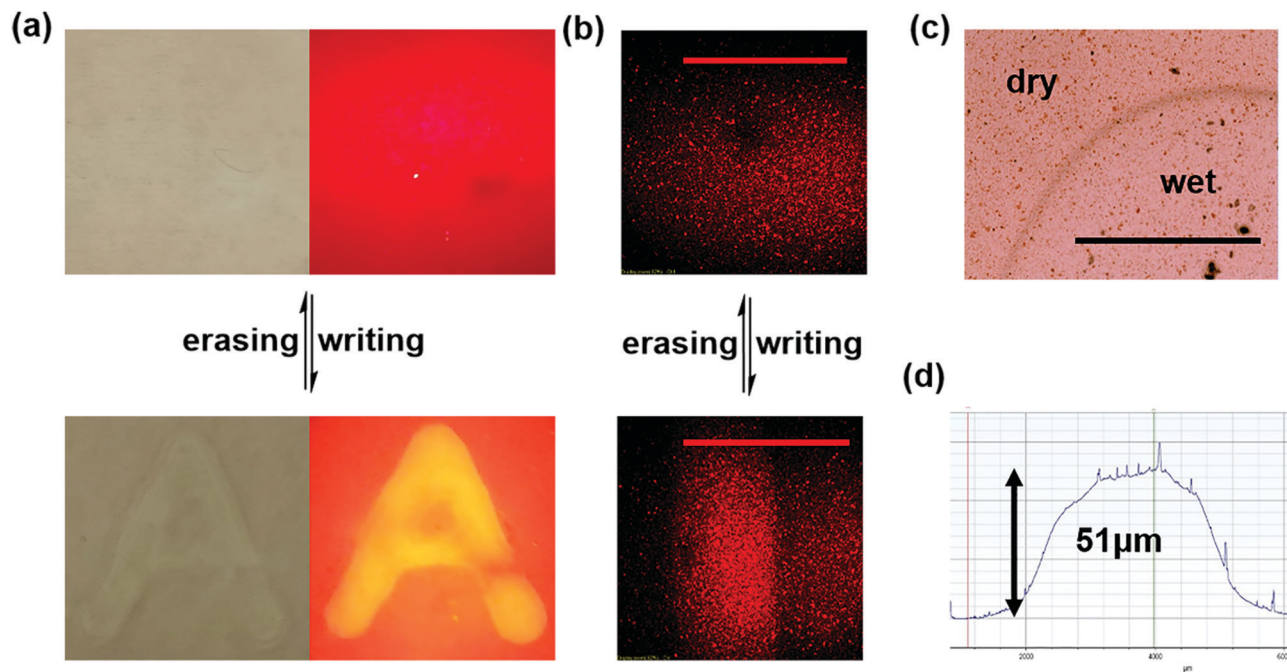
Fig. 2 (a) Wetting−dehydration photo of letter ''A'' under white light and 405 nm laser illumination. (b) 405 nm LSCM image under a wetting−dehydration process. The color is pseudo color and the scale bar is 1 mm. (c) Microscopy photos under a white light of boundary. The scale bar is 1 mm. (d) The swelling height of the wet part measured by the step profiler was 51 μm. All fluorescence photos were taken with a 500 nm filter loaded on the mobile phone.
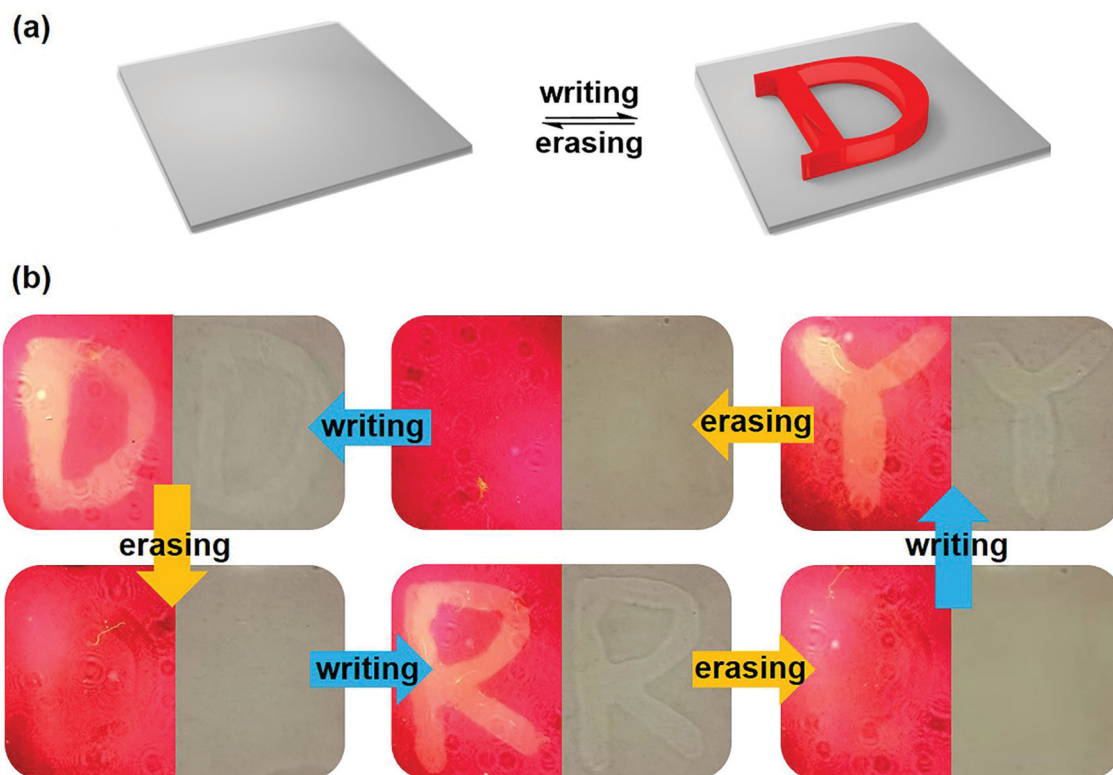

Fig. 3 (a) Simulation of the rewriting performance. (b) Fluorescence and white light photos of writing−erasing circle, the ''D''-''R''-''Y'' were displayed in turn. All fluorescence photos were taken under a 405 nm laser illumination with a 500 nm filter loaded on the mobile phone.
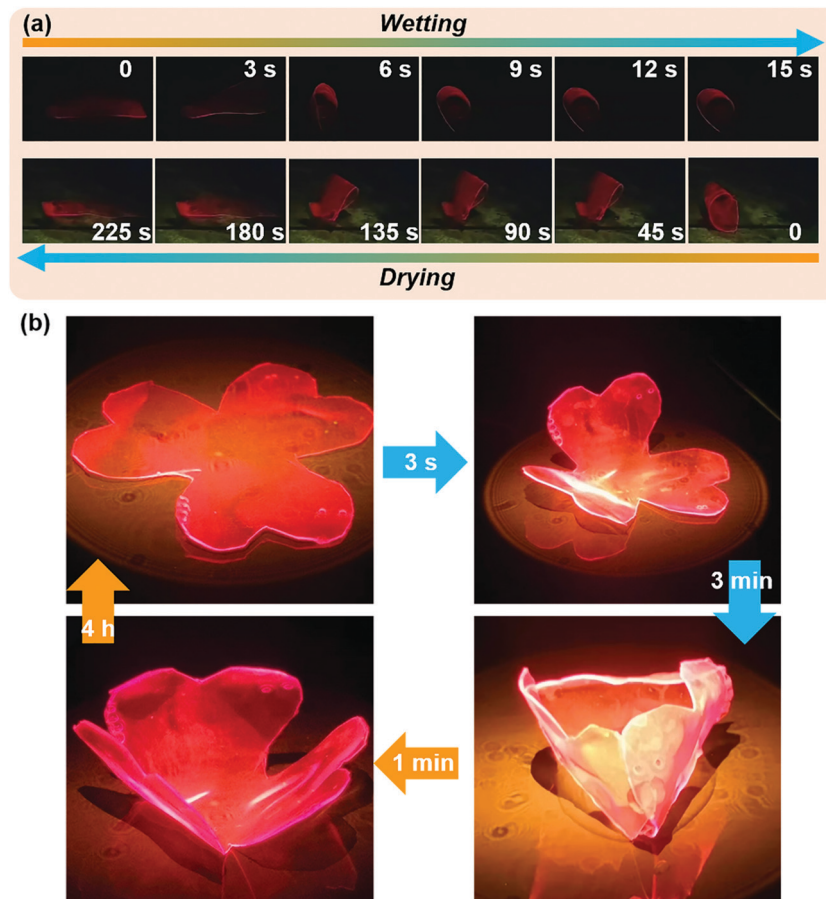
Fig. 4 (a) Water-triggered curling and unfolding process of the TCPP-polyurethane-PP bilayer film. (b) Opening and closing of the Zn-TCPP-polyurethane-PP clover under wetting (blue arrow) and drying (orange arrow). All fluorescence photos were taken under a 405 nm laser illumination with a 500 nm filter loaded on the mobile phone.

turns light red at noon, and turns crimson in the evening; the color changes three times a day. This interesting natural phenomenon encourages us to use artificial materials to replicate coordinated appearance change by environmental stimulus response. To mimic these behaviors of organisms, a bilayer water-triggered bending film was designed and prepared. A soft polypropylene (PP) film was selected as the substrate of the bilayer that could neither be corroded by THF at room temperature nor deform at 80 °C. The MOF-PU gel was coated on the PP film and dried in a vacuum oven at 80 °C. Water can cause the expansion of MOF-PU film but had no impact on PP, resulting in the bending for PP and MOF-PU composite. With the PP layer facing up, one end of the bilayer material was fixed, then water was dripped under the film. The film was curling rapidly after exposure to water. In the subsequent vacuum dehydration process, the film recovered from curling to flattening (Fig. 4(a)). Inspired by this, a water controlled opening–closing clover was designed to further demonstrate the application value of the MOF-PU gel. After adding water, the clover bent and closed rapidly, along with the fluorescence intensity increase. After short dehydration, the clover also opened accordingly, and the fluorescence intensity decreased. (Fig. 4(b)) Obviously, the opening and closing of clover could

be controlled by addition of water and dehydration, which is of great significance in biological simulation. To a certain degree, this composite material might be of fundamental value for application in soft robots.

Conclusions

In summary, we demonstrate experimentally a water-triggered dual-response smart gel with reversible fluorescence variation and shape deformation by combining Zn-TCPP MOFs with a type of polyurethane. The Zn-TCPP/polyurethane hybrid gel exhibited synergistic dynamic fluorescence and reconfigurable patterns during a dynamic wetting–drying process, which could even be observed directly by the naked eye. Moreover, the flower-like opening and closing of an artificial actuator with simultaneous fluorescence variation during a dynamic wetting process could be realized by using a soft polypropylene (PP) film as the substrate. To sum up, the developed dual response gel has the advantages of simple synthesis, low price, good repeatability and fast response speed. Besides, water as a common substance is very meaningful to regulate the properties of MOFs. This work provides an effective strategy which

could reversibly manipulate MOF properties and expand its application.

Author contributions

Conflicts of interest

There are no conflicts to declare.

Acknowledgements

Notes and references

1 J. S. Sparks, R. C. Schelly, W. L. Smith, M. P. Davis, D. Tchernov, V. A. Pieribone and D. F. Gruber, The covert world of fish biofluorescence: A phylogenetically widespread and phenotypically variable phenomenon, *PLoS One*, 2014, **9**, e83259.

2 S. Reiter, P. Hulsdunk, T. Woo, M. A. Lauterbach, J. S. Eberle, L. A. Akay, A. Longo, J. Meier-Credo, F. Kretschmer, J. D. Langer, M. Kaschube and G. Laurent, Elucidating the control and development of skin patterning in cuttlefish, *Nature*, 2018, **562**, 361–366.

3 L. Wang, A. M. Urbas and Q. Li, Nature-inspired emerging chiral liquid crystal nanostructures: From molecular self-assembly to DNA mesophase and nanocolloids, *Adv. Mater.*, 2020, **32**, 1801335.

4 C. A. McLean, A. Lutz, K. J. Rankin, A. Elliott, A. Moussalli and D. Stuart-Fox, Red carotenoids and associated gene expression explain colour variation in frillneck lizards, *Proc. Biol. Sci.*, 2019, **286**, 20191172.

5 Z.-C. Ma, X.-Y. Hu, Y.-L. Zhang, X.-Q. Liu, Z.-S. Hou, L.-G. Niu, L. Zhu, B. Han, Q.-D. Chen and H.-B. Sun, Smart compound eyes enable tunable imaging, *Adv. Funct. Mater.*, 2019, **29**, 1903340.

6 C. L. Huffard, Locomotion by abdopus aculeatus (cephalopoda: octopodidae): Walking the line between primary and secondary defences, *J. Exp. Biol.*, 2006, **209**, 3697–3707.

7 S. Wei, Z. Li, W. Lu, H. Liu, J. Zhang, T. Chen and B. Z. Tang, Multicolor fluorescent polymeric hydrogels, *Angew. Chem., Int. Ed.*, 2021, **60**, 8608–8624.

8 D. P. Karothu, J. Weston, I. T. Desta and P. Naumov, Shape-memory and self-healing effects in mechanosalient molecular crystals, *J. Am. Chem. Soc.*, 2016, **138**, 13298–13306.

9 S. Hayashi and T. Koizumi, Elastic organic crystals of a fluorescent π-conjugated molecule, *Angew. Chem., Int. Ed.*, 2016, **128**, 2751–2754.

10 A. K. Saini, K. Natarajan and S. M. Mobin, A new multi-talented azine ligand: Elastic bending, single-crystal-to-single-crystal transformation and a fluorescence turn-on Al(III) sensor, *Chem. Commun.*, 2017, **53**, 9870–9873.

11 E. P. Kenny, A. C. Jacko and B. J. Powell, Mechanomagnetics in elastic crystals: Insights from [Cu(acac)2], *Angew. Chem., Int. Ed.*, 2019, **58**, 15082–15088.

12 X. Yan, F. Wang, B. Zheng and F. Huang, Stimuli-responsive supramolecular polymeric materials, *Chem. Soc. Rev.*, 2012, **41**, 6042–6065.

13 Z. Chi, X. Zhang, B. Xu, X. Zhou, C. Ma, Y. Zhang, S. Liu and J. Xu, Recent advances in organic mechanofluorochromic materials, *Chem. Soc. Rev.*, 2012, **41**, 3878–3896.

14 P. Wei, J. X. Zhang, Z. Zhao, Y. Chen, X. He, M. Chen, J. Gong, H. H. Sung, I. D. Williams, J. W. Y. Lam and B. Z. Tang, Multiple yet controllable photoswitching in a single AIEgen system, *J. Am. Chem. Soc.*, 2018, **140**, 1966–1975.

15 C. N. Zhu, T. Bai, H. Wang, J. Ling, F. Huang, W. Hong, Q. Zheng and Z. L. Wu, Dual-encryption in a shape-memory hydrogel with tunable fluorescence and reconfigurable architecture, *Adv. Mater.*, 2021, **33**, 2102023.

16 S. Wu, H. Shi, W. Lu, S. Wei, H. Shang, H. Liu, M. Si, X. Le, G. Yin, P. Theato and T. Chen, Aggregation-induced emissive carbon dots gels for octopus-inspired shape/color synergistically adjustable actuators, *Angew. Chem., Int. Ed.*, 2021, **60**, 21890–21898.

17 J. S. Kahn, L. Freage, N. Enkin, M. A. Garcia and I. Willner, Stimuli-responsive DNA-functionalized metal–organic frameworks (MOFs), *Adv. Mater.*, 2017, **29**, 1602782.

18 M. K. Tsang, G. Bai and J. Hao, Stimuli responsive upconversion luminescence nanomaterials and films for various applications, *Chem. Soc. Rev.*, 2015, **44**, 1585–1607.

19 Y. Zhang, S. Yuan, G. Day, X. Wang, X. Yang and H.-C. Zhou, Luminescent sensors based on metal–organic frameworks, *Coord. Chem. Rev.*, 2018, **354**, 28–45.

20 X.-Y. Xu, X. Lian, J.-N. Hao, C. Zhang and B. Yan, A double-stimuli-responsive fluorescent center for monitoring of food spoilage based on dye covalently modified EuMOFs: From sensory hydrogels to logic devices, *Adv. Mater.*, 2017, **29**, 1702298.

21 K. Li, K. He, Q. Li, B. Xia, Q. Wang and Y. Zhang, Crystal structure and photoluminescence properties of two barium(II) MOFs, *Chem. Res. Chin. Univ.*, 2018, **34**, 700–704.

22 A. Kirchon, L. Feng, H. F. Drake, E. A. Joseph and H.-C. Zhou, From fundamentals to applications: A toolbox for robust and multifunctional MOF materials, *Chem. Soc. Rev.*, 2018, **47**, 8611–8638.

23 H. Furukawa, K. E. Cordova, M. O'Keeffe and O. M. Yaghi, The chemistry and applications of metal–organic frameworks, *Science*, 2013, **341**, 1230444.

24 L. E. Kreno, K. Leong, O. K. Farha, M. Allendorf, R. P. Van Duyne and J. T. Hupp, Metal–organic framework materials as chemical sensors, *Chem. Rev.*, 2012, **112**, 1105–1125.

25 S. A. Diamantis, A. Margariti, A. D. Pournara, G. S. Papaefstathiou, M. J. Manos and T. Lazarides, Luminescent metal–organic frameworks as chemical sensors: Common pitfalls and proposed best practices, *Inorg. Chem. Front.*, 2018, **5**, 1493–1511.

26 W. P. Lustig, S. Mukherjee, N. D. Rudd, A. V. Desai, J. Li and S. K. Ghosh, Metal–organic frameworks: Functional luminescent and photonic materials for sensing applications, *Chem. Soc. Rev.*, 2017, **46**, 3242–3285.

27 Y. Cui, Y. Yue, G. Qian and B. Chen, Luminescent functional metal–organic frameworks, *Chem. Rev.*, 2012, **112**, 1126–1162.

28 F.-Y. Yi, D. Chen, M.-K. Wu, L. Han and H.-L. Jiang, Chemical sensors based on metal–organic frameworks, *ChemPlusChem*, 2016, **81**, 675–690.

29 X. Zhang, K. S. Lovejoy, A. Jasanoff and S. J. Lippard, Water-soluble porphyrins as a dual-function molecular imaging platform for MRI and fluorescence zinc sensing, *Proc. Natl. Acad. Sci. U. S. A.*, 2007, **104**, 10780–10785.

30 Y. Weng, F. Yue, Y. Zhong and B. Ye, A copper(II) ion-selective on–off-type fluoroionophore based on zinc porphyrin–dipyridylamino, *Inorg. Chem.*, 2007, **46**, 7749–7755.

31 X. Wang, C. Chu, Y. Wu, Y. Deng, J. Zhou, M. Yang, S. Zhang, D. Huo and C. Hou, Synthesis of Yttrium(III)-based rare-earth metal–organic framework nanoplates and its applications for sensing of fluoride ions and pH, *Sens. Actuators, B*, 2020, **321**, 128455.

32 R. Yang, K. Li, K. Wang, F. Zhao, N. Li and F. Liu, Porphyrin assembly on β-cyclodextrin for selective sensing and detection of a zinc ion based on the dual emission fluorescence ratio, *Anal. Chem.*, 2003, **75**, 612–621.

33 C. Li, X. Zhang, L. Qiao, Y. Zhao, C. He, S. Huan, L. Lu, L. Jian, G. Shen and R. Yu, Naphthalimide–porphyrin hybrid based ratiometric bioimaging probe for Hg^{2+}: Well-resolved emission spectra and unique specificity, *Anal. Chem.*, 2009, **81**, 9993–10001.

34 Y. Chen and H. Jiang, Porphyrinic metal–organic framework catalyzed Heck-reaction: Fluorescence "turn-on" sensing of Cu(II) ion, *Chem. Mater.*, 2016, **28**, 6698–6704.

35 S. Walter, S. Susanne, W. Simon, S. Herbert, F. Clemens, G. Claudia, E. G. Alwin, K. Rainer and J. R. Hans, Intraoperative detection of malignant gliomas by 5-aminolevulinic acid-induced porphyrin fluorescence, *Neurosurgery*, 1998, **42**, 518–526.

36 C. Zhang, S. Zhang, Y. Yan, F. Xia, A. Huang and Y. Xian, Highly fluorescent polyimide covalent organic nanosheets as sensing probes for the detection of 2,4,6-trinitrophenol, *ACS Appl. Mater. Interfaces*, 2017, **9**, 13415–13421.

37 S. Tao, G. Li and H. Zhu, Metalloporphyrins as sensing elements for the rapid detection of trace TNT vapour, *J. Mater. Chem.*, 2006, **16**, 4521–4528.

38 J. Yang, Z. Wang, K. Hu, Y. Li, J. Feng, J. Shi and J. Gu, Rapid and specific aqueous-phase detection of nitroaromatic explosives with inherent porphyrin recognition sites in metal–organic frameworks, *ACS Appl. Mater. Interfaces*, 2015, **7**, 11956–11964.

39 Y. Ma, H. Su, X. Kuang, X. Li, T. Zhang and B. Tang, Heterogeneous nano metal–organic framework fluorescence probe for highly selective and sensitive detection of hydrogen sulfide in living cells, *Anal. Chem.*, 2014, **86**, 11459–11463.

40 X. Li, J. Hou, R. Guo, Z. Wang and J. Zhang, Constructing unique cross-sectional structured mixed matrix membranes by incorporating ultrathin microporous nanosheets for efficient CO_2 separation, *ACS Appl. Mater. Interfaces*, 2019, **11**, 24618–24626.

41 V. Freger, Swelling and Morphology of the skin layer of polyamide composite membranes: An atomic force microscopy study, *Environ. Sci. Technol.*, 2004, **38**, 3168–3175.

42 B. Hoffmann, J. Kressler, G. Stöppelmann, C. Friedrich and G.-M. Kim, Rheology of nanocomposites based on layered silicates and polyamide-12, *Colloid Polym. Sci.*, 2000, **278**, 629–636.

43 S. Gayathri, R. Vasanthi, M. Vanjinathan and R. Kumaran, Photophysical and electrochemical studies of 4-dicyanomethylene 2,6-dimethyl-4h-pyran (DDP) dye with amides in water, *J. Fluoresc.*, 2018, **28**, 1379–1391.

44 R. Kumaran and P. Ramamurthy, Photophysical studies on the interaction of formamide and alkyl substituted amides with photoinduced electron transfer (PET) Based acridine-dione dyes in water, *J. Fluoresc.*, 2011, **21**, 2165.

45 S. Wang, J. Chen, X. Feng, G. Shi, J. Zhang and X. Wan, Conformation shift switches the chiral amplification of helical copoly(phenylacetylene)s from abnormal to normal "sergeants-and-soldiers" effect, *Macromolecules*, 2017, **50**, 4610–4615.